Surface Plasmon Resonance Studies of Gold and Silver Nanoparticles Linked to Gold and Silver Substrates by 2-Aminoethanethiol and 1,6-Hexanedithiol

ARTICLE *in* THE JOURNAL OF PHYSICAL CHEMISTRY B · NOVEMBER 2001

Impact Factor: 3.3 · DOI: 10.1021/jp011424y

Surface Plasmon Resonance Studies of Gold and Silver Nanoparticles Linked to Gold and Silver Substrates by 2-Aminoethanethiol and 1,6-Hexanedithiol

E. Hutter,[†] J. H. Fendler,*[,†,‡] and D. Roy*[,§]

Center for Advanced Materials Processing and Department of Physics, Clarkson University, Potsdam, New York 13699

Received: April 17, 2001; In Final Form: August 6, 2001

Self-assembled monolayers (SAMs) of 2-aminoethanethiol (AET) or 1,6-hexanedithiol (HDT) are formed on Au and Ag substrates, and colloidal Au (13.6 ± 2.0 nm diameter) and Ag (30.0 ± 10 nm diameter) nanoparticles are deposited onto these SAM surfaces. The resulting multilayered nanostructures, prepared with different combinations of the substrate, SAM, and nanoparticles, are studied with surface plasmon resonance (SPR) measurements. Under certain circumstances, the SPR sensitivity of the bare metal is considerably enhanced by the presence of the metal particles. Both the occurrence and the degree of this effect depend strongly on the choice of the combination of materials in the multilayered system. The substrate/SAM/nanoparticles systems that exhibit the enhanced SPR sensitivity include Au/AET/Au, Au/HDT/Au, Au/AET/Ag, and Ag/AET/Ag. On the other hand, the effects of the nanoparticles are relatively week for Au/HDT/Ag, Ag/HDT/Ag, Ag/AET/Au, and Ag/HDT/Au. The observed system-selective nature of the nanoparticle induced SPR enhancement is discussed using Fresnel equations in a six-phase model. The results demonstrate how the interactions within and among the different components of a nanoparticle based SPR sensor affect the performance of such a sensor. These results also demonstrate the potential utility of the SPR technique in the investigation of structural and optical properties of self-assembled nanostructured materials.

1. Introduction

The SPR technique is now routinely used in a wide variety of chemical and biological sensors.[1−5] Typically, the technique involves optical excitation of surface plasmon polariton (SPP) waves on a gold or silver film employing the Kretschmann configuration for attenuated total reflection (ATR).[6−11] The ATR signal (reflectivity) R is measured as a function of the incidence angle θ_0 of the probe light beam. At a fixed optical wavelength, the $(R - \theta_0)$ plot (SPR plot) typically exhibits an approximately Lorentzian behavior,[6] with a reflectivity minimum R^p at the SPR angle θ_0^p. When a thin film of the experimental sample is adsorbed onto the SPP-supporting substrate metal, the SPR plot changes in response to the presence of the sample. Generally, such changes include a shift in the value of θ_0^p, as well as changes in the differential reflectivity $\Delta R/R$ and the width Γ_w. Here, $\Delta R = R - R^p$, and R is the reflectivity at the initial (critical) angle in an angle-scanned SPR experiment. The thickness and the dielectric function of the sample can be measured by analyzing these features of such SPR plots collected at different wavelengths.[8] For SPR-based sensor applications, the latter information is then related to the amount and chemical properties of the sample. Recently, it has been demonstrated that under certain conditions, the sensitivity of such SPR sensors can be considerably enhanced by incorporating a layer of Au nanoparticles of ∼10−60 nm diameter in the SPR device.[12−15] In this approach, a self-assembled monolayer (SAM) of a thiol or dithiol is formed on the SPP substrate, and the nanoparticle layer is adsorbed onto the SAM. Depending on the experimental conditions, the adsorbed nanoparticles can collectively or selectively alter the three signature SPR features (θ_0^p, Γ_w, and $\Delta R/R$) of the substrate/SAM system, thereby enhancing the detection sensitivity of the SPR device.[12,13] This observation is particularly relevant for potential applications of nanoparticles in the development of high sensitivity SPR sensors. The underlying mechanism of the observed nanoparticle induced SPR enhancement is governed by various interactions among and within the substrate-, SAM-, and particle-layers of such a device.[15] However, the details of these interactions are not fully understood at the present time, and this is an important issue in terms of further development of such high-performance SPR sensors. Furthermore, the observation of the nanoparticle enhanced SPR phenomenon has opened up the possibility of using the SPR technique as a probe of structural and optical properties of chemically self-assembled two-dimensional (2-D) and three-dimensional (3-D) nanostructured composite materials in general.[16] The present work is centered on these issues of nanoparticle enhanced SPR.

In a brief preliminary account of the present work, we have studied the role of the substrate metal (Au and Ag) in the SPR behavior of multilayer composites involving Au nanoparticles stabilized by HDT.[15] In the current report, we consider more generalized aspects of metal nanoparticle modified SPR. Here, we investigate the relative roles of the nanoparticle metal, substrate metal, and the spacer SAM between the substrate- and particle-layers. We assemble different substrates, SAMs and nanoparticles in multilayered films, and probe different combinations of the materials in the composite system with SPR experiments. We study Au and Ag nanoparticles on both Au and Ag substrates. To attach the particles with the substrate, we use two different SAMs, AET, and HDT.[17] By changing

* To whom correspondence should be addressed.
[†] Center for Advanced Materials Processing, Clarkson University, Box 5814.
[‡] E-mail: fendler@clarkson.edu.
[§] Physics Department, Clarkson University, Box 5820. E-mail: samoy@clarkson.edu.

10.1021/jp011424y CCC: $20.00
Published on Web 10/19/2001

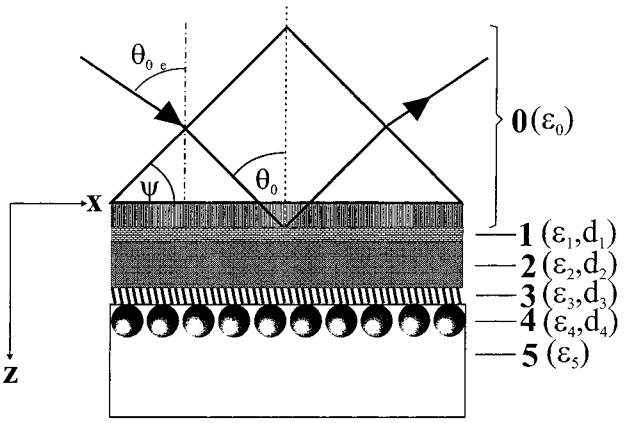

Figure 1. Schematic diagram of the nanoparticle-based multilayer SPR device (not drawn to scale) used in this work. The incident and reflected lights are in the *xz*-plane of the coordinate system shown. Layers 1, 2, 3, and 4 represent a binding film of Cr, the SPP substrate (Au or Ag), a SAM (AET or HDT), and the nanoparticles (Au or Ag), respectively. The dielectric functions ϵ_m and thicknesses d_m of the different layers ($m = 0-5$) of the SPR device are noted in the Figure.

the SAM, from AET to HDT, the particles−SAM binding interactions are changed from electrostatic to covalent. The optical properties, including the localized surface plasmon (LSP) characteristics[18−21] of the particles are studied prior to their incorporation in the SPR system by using optical absorption spectroscopy.[18] The morphologies of the nanoparticle layers in the SPR system are examined with scanning electron microscopy (SEM). The SPR data are analyzed using Fresnel equations for a general *N*-layer ($N = 3-6$) model.[22] In addition, a relatively simple phenomenological framework is presented to explain how the different components of the multilayered SPR device (and their interactions) can affect the observed SPR parameters, θ_0^{p}, Γ_{w}, and $\Delta R/R$.

2. Theory

A schematic diagram of a typical multilayer SPR device is shown in Figure 1. The dielectric function and thickness of the *m*th phase are denoted as ϵ_m and d_m, respectively, and the different phases are as follows: (0) a glass prism, refractive index matched (using a fluid) with a glass slide; (1) a thin binder layer of Cr; (2) the SPP supporting substrate film of Au or Ag; (3) a SAM of AET or HDT; (4) the nanoparticle layer, chemically linked by the SAM to the SPP substrate; (5) air. In the present work, we use three types of multilayer systems, namely, the four-phase (0125), five-phase (01235), and six-phase (012345) systems. The angle of incidence at the 0−1 interface (inside the prism) is θ_0. We refer to $\theta_{0\mathrm{e}}$ as the external incidence angle. The base angle of the prism is ψ.

To outline the working principle of the SPR device of Figure 1, we note that the Fresnel reflection coefficient for the six-phase system, determined with attenuated total reflection (ATR) in the Kretschmann configuration, has the following form:[24] $r_{012345} = S_{21}^{(6)}/S_{11}^{(6)}$, where S_{pq} is the element in the *p*th row and *q*th column of the scattering matrix $\mathbf{S}^{(6)}$ of the six-phase system. The reflectivity of this system is obtained as $R = |r_{012345}|^2$. For a general, *N*-layer system,[22]

$$\mathbf{S}^{(N)} = \mathbf{I}^{(01)}\mathbf{L}^{(1)}...\mathbf{L}^{(N-1)}\mathbf{I}^{((N-1)N)} \tag{1}$$

where $\boldsymbol{I}^{((m-1)m)}$ is the interface matrix for the $(m-1)m$ interface, and $\mathbf{L}^{(\mathrm{m})}$ is the layer matrix for the *m*th phase. The first matrix depends on the reflection and transmission coefficients of all the constituent interfaces of the multilayer structure. The second matrix depends on the thickness (d_m) of the individual layers. Explicit forms of these matrixes have been discussed in detail in previous publications[22−25] and, therefore, will not be presented here. The incident light beam couples to the SPP waves of layer 2 when the optical wavenumber k_x^{in} satisfies the condition[6,10]

$$k_x^{\mathrm{in}} \approx \tilde{\omega}\sqrt{\epsilon_0}\sin\theta_0 = \mathrm{Re}[k_x] \tag{2}$$

where $\tilde{\omega} = \omega/c = (2\pi)/\lambda$, and *c* is the velocity of light in a vacuum. $\mathrm{Re}[k_x]$ is the real part of the plasmon wavenumber k_x, the latter being continuous across the layers.[6] The *z*-component of the wave vector in medium *m* is written as $k_{mz} = [\tilde{\omega}^2\epsilon_m - k_x^2]^{1/2}$. At the wavelength (638.2 nm) used in our present study, ϵ_m is real for the nonmetallic phases where $m = 0$, 3. and 5, and ϵ_{m} is complex for the metallic phases where $m = 1$, 2, and 4.[26,27] Thus, ϵ_m ($m = 1, 2, 4$) $= \epsilon_{mr} + i\epsilon_{mi}$, where ϵ_{mr} and ϵ_{mi} are the real and imaginary parts of ϵ_m, respectively, and $i = \sqrt{-1}$.

The wave vector components k_x and k_{mz} are different from their corresponding unperturbed values k_x^0 and k_{mz}^0, where the latter terms are defined for SPP oscillations at the interface of two semi-infinite media 2 and 5. Here, $k_{mz}^0 = [\tilde{\omega}^2\epsilon_m - (k_x^0)^2]^{1/2}$, and[6,28−30]

$$k_x^0 = \tilde{\omega}[(\epsilon_2\epsilon_5)/(\epsilon_2 + \epsilon_5)]^{1/2} \tag{3}$$

Three main factors are responsible for changing the SPP wavenumber from k_x^0 to k_x: finite width of layer 2 (as well as its association with layers 0 and 1), presence of layer 3, and presence of layer 4. Phenomenologically, contributions of these three factors to the net change of k_x^0 can be denoted as $\Delta k_x^{(2)}$, $\Delta k_x^{(3)}$, and $\Delta k_x^{(4)}$, respectively, so that[26]

$$k_x \approx k_x^0 + \Delta k_x^{(2)} + \Delta k_x^{(3)} + \Delta k_x^{(4)} \tag{4}$$

Equation 1 presents the general form of the $R - \theta_0$ relationship for the multilayer SPR system. Numerical solution of this equation will provide the analysis of the experimental results presented later. In such a calculation, however, it is difficult to show how the three above-mentioned effects (shown in eq 4 as separate contributions of layers 2, 3, and 4) are correlated with the observed features of the experimental $R - \theta_0$ data. These correlations can be noted by deriving an approximate analytical formula for *R* from eq 1, on the basis of the assumptions of eq 4.[26] In this latter approach, relatively simple expressions can be derived for $\Delta k_x^{(2)}$ and $\Delta k_x^{(3)}$ of eq 4:

$$\Delta k_x^{(2)} = \frac{2\tilde{\omega}r_{02}^0\,\alpha_2^0}{|\epsilon_{2\mathrm{r}}| + \epsilon_5}\left(\frac{|\epsilon_{2\mathrm{r}}|\epsilon_5}{|\epsilon_{2\mathrm{r}}| - \epsilon_5}\right)^{3/2} \tag{5}$$

$$\alpha_2^0 = \exp\left[\frac{-2\tilde{\omega}d_2|\epsilon_{2\mathrm{r}}|}{(|\epsilon_{2\mathrm{r}}| - \epsilon_5)^{1/2}}\right] \tag{6}$$

$$\Delta k_x^{(3)} = \frac{(\tilde{\omega}^2 d_3)(|\epsilon_{2\mathrm{r}}| + \epsilon_3)(\epsilon_3 - \epsilon_5)}{\eta_{25}\epsilon_3} \tag{7}$$

$$\eta_{25} = \frac{(|\epsilon_{2\mathrm{r}}| - \epsilon_5)^2(|\epsilon_{2\mathrm{r}}| + \epsilon_5)}{(|\epsilon_{2\mathrm{r}}|\epsilon_5)^{3/2}} \tag{8}$$

where r_{02}^0 represents the value of r_{02} evaluated at $k_x = k_x^0$; α_2^0 and η_{25} are dimensionless parameters. The wavenumber shift $\Delta k_x^{(4)}$ can be obtained from eq 8 by replacing d_3 and ϵ_3 with d_4

and ($\epsilon_{4r} + \epsilon_{4i}$), respectively.[26] Note that $\Delta k_x^{(3)}$ is real, but both $\Delta k_x^{(2)}$ and $\Delta k_x^{(4)}$ are complex. Incorporating eqs 5−8, and their underlying assumptions in eq 1, the reflectivity of the (012345) multilayer system can be written in the following Lorentzian form:[15,24−26]

$$R(012345) = |r_{012345}|^2 \approx |r_{02}^0|^2\left[1 - \frac{4\Gamma_{in}\Gamma_{rad}}{\{k_x^{in} - (\Gamma^* + \Gamma_+'')\}^2 + \Gamma_w^2}\right] \quad (9)$$

where Γ_w is the width of the SPR plot, $\Gamma_w = \Gamma_{in} + \Gamma_{rad}$; Γ_{in} and Γ_{rad} correspond to internal and radiation damping of SPR, respectively; $\Gamma^* = \mathrm{Re}[k_x^0]$; $\Gamma_+'' = \Gamma_+' + \mathrm{Re}[\Delta k_x^{(4)}]$; $\Gamma_+' = \Gamma_+ + \Delta k_x^{(3)}$; and $\Gamma_+ = \mathrm{Re}[\Delta k_x^{(2)}]$. In addition,

$$\Gamma_{in} = \mathrm{Im}[k_x^0] + \mathrm{Im}[k_x^{(4)}] \quad (10)$$

$$\Gamma_{rad} = \mathrm{Im}[\Delta k_x^{(2)}] \quad (11)$$

The real and imaginary parts of the complex quantities in the above expressions are labeled with Re and Im, respectively. Equation 9 indicates how the SPR plot of a bare Au or Ag film (0125 system) would change upon the incorporation of the SAM (01235 system) and the nanoparticles (012345 system). For the (01235) structure, where $d_3 = d_4 = 0$, with $\Delta k_x^{(3)} = \Delta k_x^{(4)} = 0$, the reflectivity in eq 9 passes through a minimum when the incidence angle satisfies the condition, $k_x^{in}(\theta_0 = \theta_0^p) = \Gamma^* + \Gamma_+$. Upon the adsorption of the SAM ($d_3 \neq 0$, $k^{(3)} \neq 0$, $d_4 = 0$ and $k^{(4)} = 0$), the SPR angle shifts to a new value, $\theta_0^{p'}$, when the condition for the reflectivity minimum, $k_x^{in}(\theta_0 = \theta_0^{p'}) = \Gamma^* + \Gamma_+ + \Delta k_x^{(3)}$, is satisfied.[9] At the same time, if the SAM interacts with the SPP substrate, leading to a change in ϵ_2, then the terms, Γ^* and $\Delta k_x^{(2)}$ would also change, giving rise to their additional shifts in the SPR angle.[26] Furthermore, Γ_{in} and Γ_{rad}, and hence, Γ_w, depend on ϵ_0 and ϵ_2 (as well as on ϵ_4, ϵ_5, and d_4). Thus, a change of ϵ_2 would also change the SPR width Γ_w. The same considerations would apply to the (012345) case when the nanoparticle layer is introduced, and d_3, d_4, $\Delta k_x^{(3)}$, and $\Delta k_x^{(4)}$ all have nonzero values. The new SPR angle for the six-phase system would follow from the condition for the reflectivity minimum $k_x^{in}(\theta_0 = \theta_0^{p'}) = \Gamma^* + \Gamma_+ + \Delta k^{(3)} + \mathrm{Re}[\Delta k_x^{(4)}]$. If ϵ_2 changes due to direct or SAM-mediated interactions between the SPP substrate and the nanoparticles, the SPR shift in the SPR angle would contain a contribution of this effect. The SPR width would be affected by the nanoparticles due to the presence of the term, $\mathrm{Im}[\Delta k_x^{(4)}]$ in Γ_w. An additional change to the SPR width would appear if ϵ_2 changes due to substrate-nanoparticle interactions. It should be noted that eq 9, being an approximate form of eq 1, is valid only in the neighborhood of the resonance angle. However, eq 9 clearly brings out the correlations among the experimental parameters and the different features of SPR plots, while these correlations are not obvious in the full reflectivity formulas obtained from eq 1.

The introduction of the nanoparticles to the SPR device (the transition from the 01235 to 012345 systems) introduces the dielectric function ϵ_4 in the expression of R. According to the effective medium approximation (EMA),[27] ϵ_4 is a function of ϵ_5 and ϵ_M^{np}, where the latter term represents the dielectric function of a nanoparticle of metal M (M ≡ Au or Ag in this work). The value of ϵ_M^{np} depends on the localized surface plasmon (LSP) characteristics of the given nanoparticle. Near the LSP resonance wavelength (frequency), ϵ_{np} can be very large, and such wavelength-dependent variations of ϵ_M^{np} can affect ϵ_4. Thus, it is the inclusion of ϵ_M^{np} in the expression of R that correlates R with the LSP properties of the nanoparticles-in addition to the SPP properties of the substrate (through k_x). However, due to interactions with the neighboring SPP-supporting metal (and the SAM), ϵ_M^{np} is expected to be different from the ϵ_M^{np} of an isolated nanoparticle.[15,26] Furthermore, as discussed above, ϵ_2 of the SPP substrate can also change because of substrate-nanoparticle interactions. The strength and details of these interactions are determined by the electronic properties of the interacting partners, that is, by the LSP and SPP characteristics of the nanoparticles and the substrate, respectively. In other words, the effective values of ϵ_M^{np} (or ϵ_4) and ϵ_2 sampled in the SPR experiment are results of direct or SAM-mediated LSP−SPP interactions in the multilayer SPR device. The choice of combination for the nanoparticle and substrate metals and the spacer SAM should play an important role in determining the details of such interactions. Consequently, if the previously observed[12−15] nanoparticle induced SPR enhancement is a result of such LSP−SPP interactions, this enhancement would depend on the above-mentioned choice of materials. In section 4 of the present report, we demonstrate that this indeed is the case for metal nanoparticle modified SPR of Au and Ag.

3. Experimental Section

Materials. Commercially available 1,6-hexanedithiol (Fluka), gold chloride trihydrate, sodium citrate, EDTA, sodium oleate (Sigma), hexane (95%, anhydrous), magnesium chloride, sulfuric acid, hydrogen peroxide (30%), sodium hydroxide, sodium Chloride (Fisher), silver nitrate (Spectrum, Chemical MFG), chrome-plated tungsten rods (CRW−2 × 0.07 in., R. D. Mathis Company), gold shots (≤0.35 mm, semispherical Premion, 99.999%, ALFA AESAR) silver shots (2−3 mm, Premion, 99.999%, ALFA AESAR), Fisher finest Premium Microscope slides (BK7, 3 in. × 1 in., Fisher Scientific), and a nylon bottle-top filter system with the pore size of 0.2 μm (Corning) were used as received. Ultrapure water was obtained from a Millipore Milli-QTM system provided with a Milli-pak filter of 0.22 μm pore size at the outlet.

Preparation and Phase-Transfer of Au and Ag Nanoparticles. The colloidal gold particles were prepared by citrate reduction of $HAuCl_4$, as reported previously.[31] Briefly, 200 mL of 0.01% $HAuCl_4$ was brought to boil, then 7 mL of 1% sodium citrate was added under vigorous stirring. The solution was allowed to cool to room temperature and filtered through a 0.2 μm pore size nylon bottle-top filter system. The phase transfer into hexane was accomplished by vigorous stirring of 20 mL of hexane, 20 mg of sodium oleate, and 20 mL of the colloidal gold dispersion for 2 h, and subsequent adding of 0.25 g $MgCl_2$ in 3 mL water. In 4 h of standing, the phases became separated and the gold nanoparticles were transferred into the organic upper phase, hexane.[31]

The colloidal silver particles were prepared by reduction of $AgNO_3$ by EDTA, as reported previously.[31] Briefly, 200 mL of 1.6×10^{-4} M aqueous solution of EDTA and 4 mL of 0.1 M aqueous solution of NaOH was brought to boil, then 1 mL of 2.6×10^{-2} M aqueous solution of $AgNO_3$ was added under vigorous stirring. The solution was allowed to cool and was filtered. The phase transfer into hexane was accomplished by vigorous stirring of 20 mL of hexane, 20 mg of sodium oleate, and 20 mL of the silver colloid dispersion for 8 h, and subsequent adding of 2 g NaCl. The phases were separated after

TABLE 1: Dielectric Functions and Layer Thicknesses of Multilayered Nanostructures Involving Au Nanoparticles

system	ϵ_{2r}[a]	ϵ_{2i}[a]	ϵ_3[b]	ϵ_{4r}[b]	ϵ_{4i}[b]	d_1[c] (nm)	d_2[c] (nm)	d_3[b] (nm)	d_4[b] (nm)
sample I: 0125 (glass/Cr/Au/air)	−12.09	0.71				0.4	46.7	−	
sample I: 01235 (glass/Cr/Au/AET/air)	−11.99	0.64	2.00			0.4	47.4	0.4	
sample I: 012345 (glass/Cr/Au/AET/Au/air)	−11.99	0.64	2.00	−4.66	2.87	0.4	46.7	0.4	12.0
sample II: 0125 (glass/Cr/Ag/air)	−16.74	0.86				2.2	41.0		
sample II: 01235 (glass/Cr/Ag/AET/Air)	−7.87	0.43	0.07	−	−	2.23	41.0	0.5	
sample II: 012345 (glass/Cr/Ag/AET/Au/air)	−7.87	0.43	0.06	−2.20	6.46	2.2	41.0	0.8	13.0
sample III: 0125 (glass/Cr/Au/air)	−11.65	0.37				0.3	48.5		
sample III: 01235 (glass/Cr/Au/HDT/Air)	−11.80	0.33	2.00			0.3	48.5	0.7	
sample III: 012345 (glass/Cr/Au/HDT/Au/air)	−11.80	0.33	2.00	−8.81	2.43	0.3	48.5	0.7	16.0
sample IV: 0125 (glass/Cr/Ag/air)	−16.6	0.70	−			1.5	50.5	−	
sample IV: 01235 (glass/Cr/Ag/HDT/Air)	−12.84	0.48	2.00			1.5	50.5	0.7	
sample IV: 012345 (glass/Cr/Ag/HDT/Au/air)	−12.94	0.73	2.00	−10.64	1.08	1.5	50.5	0.7	10.0

[a] Initial input values to the numerical calculations of eq 1 are taken from ref 6. [b] From calculated fits in Figures 5 and 6. [c] Measured using a QCMB. Other known parameters used in the fits in Figures 5 and 6 are $\lambda = 632.8$ nm, $\epsilon_0 = 2.30$ (for BK glass),[33] $\epsilon_{1r} = -6.88$,[34] and $\epsilon_{1i} = 32.56$ (for Cr).[34]

4 h of standing. The silver nanoparticles were transferred into the hexane phase, and used within 12 h.

Fabrication of Gold and Silver Substrates. BK7 glass slides (refractive index = 1.51) were cleaned with freshly made piranha solution (*caution:* piranha solution should be handled with extreme care),[32] and rinsed with Nanopure water, and finally rinsed with ethanol. The Au or the Ag film was deposited by evaporation of ~ 1−2 nm of Cr followed by ~50 nm of Au or Ag at a base pressure of $\sim 10^{-7}$ mB using an Edwards AUTO 306 high vacuum deposition system. The deposition rate was 0.1−0.2 nm/s. The thickness of the chromium and gold or silver film and the deposition rate were monitored by a system consisting of a quartz crystal microbalance (QCMB), mechanically oscillating at its natural resonance frequency, 6 MHz.

Self-Assembly of HDT and AET, and Nanoparticles. The gold substrates were cleaned following the same cleaning procedure used for the glass slides. The silver substrates were washed thoroughly with water and ethanol. The clean substrates were immersed into the 1 mM ethanolic solution of 1,6-hexanedithiol (HDT) for 1 h, followed by thorough washing with ethanol and water, drying with gaseous nitrogen. The substrates were similarly immersed into an aqueous solution of 1 mM 2-aminoethanethiol (AET) overnight, followed by thorough washing with ethanol and water, drying with gaseous nitrogen. The AET covered Au or Ag substrates were exposed for about 25 min to aqueous dispersion (pH 6.8−7.5) of Au or Ag nanoparticles. The HDT covered substrates were also exposed to hexane-transferred Au and Ag nanoparticles for the same duration. For a given substrate metal (that is, for a given set of the first three base layers, 0, 1, and 2), four separate multilayer samples were prepared. For example, using the glass/Cr base structure, the following samples were prepared (denoted in terms of the substrate/SAM/nanoparticle combination): Au/AET/Au nanoparticles (sample I), Ag/AET/Au nanoparticles (sample II), Au/HDT/Au nanoparticles (sample III), Ag/HDT/Au nanoparticles (sample IV). Samples V, VI, VII, and VIII were prepared by using Ag instead of Au for the nanoparticle metal with the substrate/SAM combinations used in samples I, II, III, and IV, respectively. The results presented in Tables 1 and 2 refer to these eight multilayer samples. SEM Images of nanoparticle covered SAMs were taken on an FEG XL-30 Philips Instrument. Prior to the incorporation of the Au and Ag nanoparticles in the SPR device, the sizes of the particles were determined in the solution phase using transmission electron microscopy (TEM).

SPR Measurements. SPR measurements were performed using a home-built instrument. The glass side of the sample was brought into optical contact with the base of a 90° glass prism (of refractive index 1.5151) by a refractive index matching fluid (of refractive index 1.5180 ± 0.0005). A p-polarized light beam from a HeNe laser, at the wavelength of 632.8 nm (Hughes, 3235H-PC, 20 mW) was mounted on a computer-controlled stepping motor driven rotator (Oriel). The rotator allowed for varying the angle of incidence, and the ATR signal was detected with a silicon detector (Newport, 818-SL). As shown in Figure 1, the measured external angle (θ_{0e}) and the internal angle (θ_0) are related by $\theta_{0e} = \sin^{-1}[\sqrt{\epsilon_0}\sin(\theta_0 - \psi)] + \psi$, where $\psi = 45°$ in our experiments. All SPR reflectivities measured in the present work are plotted against θ_{0e}.

4. Results and Discussion

Optical Absorption and LSP Characteristics of Au and Ag Nanoparticles. Figure 2 shows absorption spectra of colloidal solutions of Au and Ag in water and hexane. The peaks and widths of the plots in Figure 2 follow their respective theoretically predicted behaviors, and agree with the previously reported results for similar systems.[18] For both Au (13.6 ± 2.0 mm diameter, determined by TEM) and Ag (30.0 ± 10 nm diameter, determined by TEM) nanoparticles, the absorption peaks in water coincide with those obtained in hexane, and the widths of the plots are also similar in the two solvents. This indicates that the nanoparticles, prepared in water, do not experience any significant changes of their optical properties

TABLE 2: Dielectric Functions and Layer Thicknesses of Multilayered Nanostructures Involving Ag Nanoparticles

system	ϵ_{2r}[a]	ϵ_{2i}[a]	ϵ_3[b]	ϵ_{4r}[b]	ϵ_{4i}[b]	d_1[c] (nm)	d_2[c] (nm)	d_3[b] (nm)	d_4[b] (nm)
sample V: 0125 (glass/Cr/Au/air)	−12.29	0.24				0.8	48.0		
sample V: 01235 (glass/Cr/Au/AET/Air)	−12.29	0.24	2.00			0.8	48.0	0.4	
sample V: 012345 (glass/Cr/Au/AET/Ag/air)	−5.89	0.80	2.00	−10.90	1.90	0.8	48.0	0.4	32.0
sample VI: 0125 (glass/Cr/Ag/air)	−17.11	0.79				2.1	43.0		
sample VI: 01235 (glass/Cr/Ag/AET/Air)	−8.84	0.46	0.07			2.1	43.0	0.4	
sample VI: 012345 (glass/Cr/Ag/AET/Ag/air)	−8.74	0.28	0.07	1.13	0.18	2.1	43.0	0.4	25.0
sample VII: 0125 (glass/Cr/Au/air)	−12.51	0.33				0.8	48.0		
sample VII: 01235 (glass/Cr/Au/HDT/Air)	−12.51	0.28	2.00			0.8	48.0	0.5	
sample VII: 012345 (glass/Cr/Au/HDT/Ag/air)	−7.31	0.89	2.00	−12.80	1.96	0.8	48.0	0.5	25.0
sample VIII: 0125 (glass/Cr/Ag/air)	−16.14	0.58				1.5	50.5		
sample VIII: 01235 (glass/Cr/Ag/HDT/Air)	−13.64	0.58	2.00			1.5	50.5		
sample VIII: 012345 (glass/Cr/Ag/HDT/Ag/air)	−14.44	0.75	2.00	1.07	0.01	1.5	50.5	0.7	26.0

[a] Initial input values to the numerical calculations of eq 1 are taken from ref 6. [b] From calculated fits in Figures 7 and 8. [c] Measured with a QCMB. The known parameters, λ, ϵ_0, ϵ_{1r}, and ϵ_{1i} are noted in the footnote to Table 1.

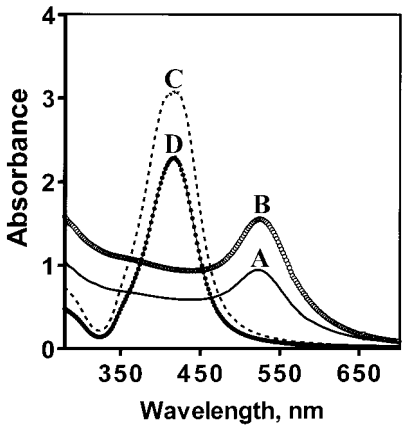

Figure 2. Absorption spectra of solutions of Au (A and B) and Ag (C and D) nanoparticles, measured using water (A and C) and hexane (B and D) as solvents.

as they are transferred in hexane for incorporation in the SPR device shown in Figure 1. As mentioned in section 2, upon their incorporation in the multilayer structure, the optical properties of the nanoparticles are expected to change due to the interactions they experience in such a configuration. This can lead to some shifts in their LSP resonance frequencies, and the direction and magnitude of such a shift would depend on the detailed chemical nature of the environment in the particle layer. As indicated in Figure 2, the LSP wavelengths (absorption peaks) for all the presently used nanoparticles in their solution phases fall well below the wavelength, 632.8 nm, used in the SPR experiments. Any interaction-induced shifts of LSP wavelengths of the nanoparticles in the SPR device are unlikely to be large enough to coincide with the above-mentioned incident wavelength. Thus, in the SPR experiments of the present work, the SPP waves of the Au or Ag film will be angle-tuned to resonate, but the LSP oscillations in the nanoparticles will be expected to remain off-resonance. In such cases, the resonant SPP characteristics of the substrate metal dominate the experimental SPR plot, while the LSP effects of the nanoparticle layer appear as changes in the effective SPP features of the multilayer system.

Morphology of Nanoparticles on SAM-Coated Substrates. In a recent work involving CdS nanoparticles stabilized by SAMS on Ag, we found evidence for crystallization in the particles layer.[25] In view of this earlier made observation, it is necessary to check if the Au and Ag colloidal particles in the present work can maintain their nanoparticle identities upon their incorporation in the SPR device. Therefore, after introducing the nanoparticle layer in the multilayer samples, the morphology of the top (nanoparticle) layer of each sample is examined with SEM. Typical SEM images of such samples are shown in Figures 3 and 4. Figure 3 shows the surfaces of samples I (Au/AET/Au, in A), II (Ag/AET/Au, in B), and IV (Ag/HDT/Au, in C). Figure 4 shows the surfaces of samples V (Au/AET/Ag), VI (Ag/AET/Ag), and VIII (Ag/HDT/Ag). These figures indicate that the Au and Ag nanoparticles do maintain their discrete particles identity (without any crystallization or large scale clustering) in the surface layer. The average diameters of the surface particles of Au and Ag are determined to be 15.6 ± 3.5 nm and 26.9 ± 5.0 nm, respectively. The fractional surface coverages of the nanoparticles, as estimated from the SEM images, are >0.95 for all samples studied in the present work. Such high particle-coverages indicate densely packed and stable films of the underlying SAMs. It should be noted here that we use the SEM data only to check the over all surface morphology of the nanoparticle covered samples. No quantitative analyses, based on these SEM images, are attempted in this work.

Results of SPR Experiments. We explored the SPR characteristics of different substrate/SAM/nanoparticle combinations using samples I−VIII, described in section 3. The $(R - \theta_{0e})$ SPR plots for these samples are presented in Figures 5−8. The symbols in each figure represent experimental data for three different cases of the multilayer structures, 0125 (circles), 01235 (triangles), and 012345 (squares). Although the external angle θ_{0e} is used in the plots, for ready reference to the expressions considered in the Theory Section, the reflectivity minima of the SPR plots will still be discussed here in terms of the internal

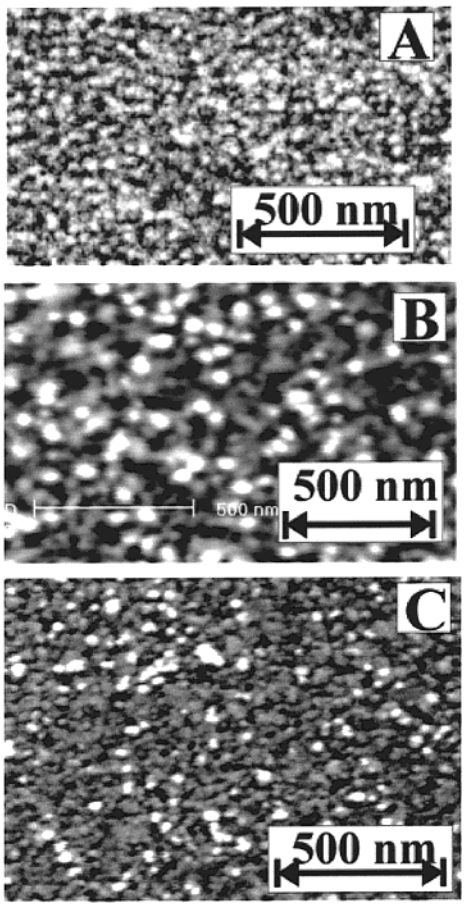

Figure 3. Sample SEM images of the top surfaces of Au nanoparticle-coated multilayer SPR systems. The SPP supporting substrate (layer 2 defined in Figure 1) is Au in A, and Ag in B and C. The chemical link (layer 3) between the substrate and the nanoparticles is AET in A and B, and HDT in C.

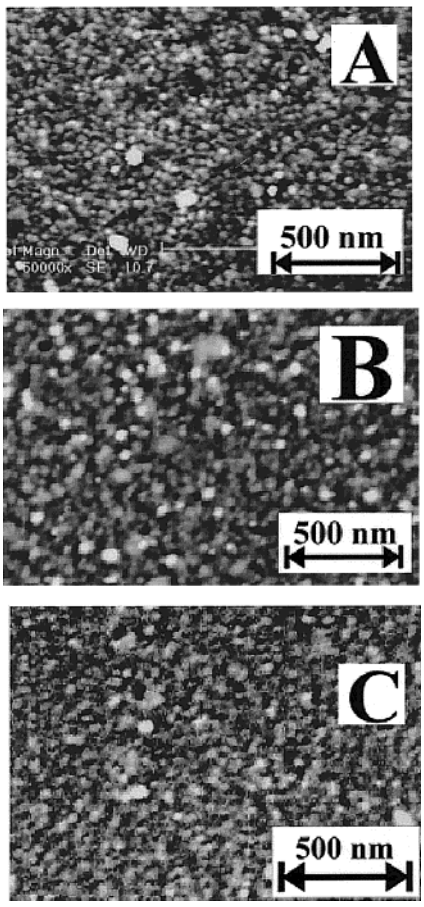

Figure 4. Sample SEM images of the top surfaces of Ag nanoparticle-coated multilayer SPR systems. The SPP supporting substrate (layer 2 defined in Figure 1) is Au in A, and Ag in B and C. The chemical link (layer 3) between the substrate and the nanoparticles is AET in A and B, and HDT in C.

resonance angle θ_0^p. We find that if we maintain $d_1 < \sim 2$ nm, and $d_2 \gg d_1$ for the initial 0125 samples, some variations in the values of d_1 and d_2 from sample to sample do not affect the relative changes introduced by the adsorption of layers 3 and 4. The solid lines through the symbols in Figures 5−8 represent calculated fits obtained from the general six-layer model described in eq 1. For each sample, the fits are obtained as follows. We measure the thickness parameters, d_1 and d_2, following the deposition of the Cr and the Au (or Ag) layers, respectively, using the QCMB method described in section 3. With these d_1 and d_2, and the known values of ϵ_0,[33] ϵ_1,[34] and ϵ_2,[6] we fit eq 1 to the SPR data for the 0125 structure. The dielectric functions are readjusted as needed to improve the fits. Next, we deposit the SAM on the Au (or Ag) film of the sample, and record the SPR data for this 01235 structure. To fit the latter set of data, an approximate d_3, based on estimation of the length of the SAM, is used as a starting input parameter for the calculations. In addition, ϵ_3 is used as a fitting parameter, and ϵ_2 is readjusted within certain small limits to refine the quality of the fit. The latter limits are estimated on the basis of our previous calculations for adsorbate induced changes in the surface dielectric functions of metals.[35−37] Subsequently, we deposit the nanoparticle layer on the SAM, and collect the SPR data for the resulting 012345 system. Next, we repeat the above-described fitting procedure, where for the initial input for d_4, we use an average diameter of the deposited nanoparticles as found in SEM images such as those of Figures 3 and 4. The parameters determined from the calculated fits to the SPR data,

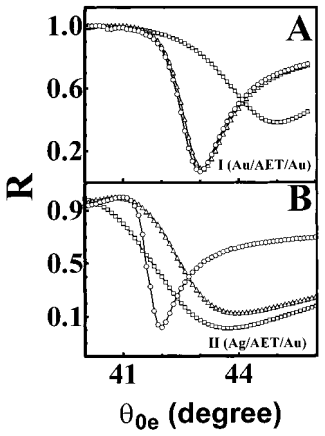

Figure 5. Experimental SPR data (symbols) and calculated fits (lines) to the data for Au (in A) and Ag (in B) substrates. The circles, triangles, and squares represent the four-phase (0125), five-phase (01235), and six-phase (012345) systems, respectively. The data in A and B refer to samples I and II described in the Experimental Section, respectively. In both parts A and B, phase 3 represents a SAM of AET, and phase 4 represents a layer of Au nanoparticles. The calculated fits represent numerical solution of the general six-layer model based on eq 1.

as well as the known parameters used for these calculations are presented in Tables 1 and 2. Note that, for the calculated fits shown in Figures 5−8, we use the general form of eq 1, and not their approximate analytical result given in eq 9. The latter expression of R will be used here to interpret the results of the general calculations. We also note that, in the framework of

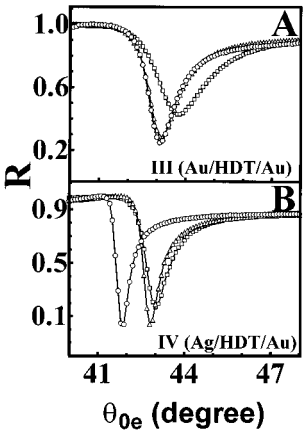

Figure 6. Experimental SPR data (symbols) and calculated fits (lines) to the data for Au (in A) and Ag (in B) substrates. The circles, triangles and squares represent the four-phase (0125), five-phase (01235), and six-phase (012345) systems, respectively. The data in A and B refer to samples III and IV described in the Experimental Section, respectively. In both parts A and B, phase 3 represents a SAM of HDT, and phase 4 represents a layer of Au nanoparticles. The theoretical fits represent results of numerical calculations using eq 1.

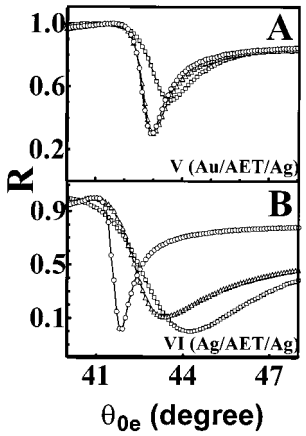

Figure 7. Experimental SPR data (symbols) and calculated fits (lines) to the data for Au (in A) and Ag (in B) substrates. The circles, triangles and squares represent the four-phase (0125), five-phase (01235), and six-phase (012345) systems, respectively. The data in A and B refer to samples V and VI described in the Experimental Section, respectively. In both parts A and B, phase 3 represents a SAM of AET, and phase 4 represents a layer of Ag nanoparticles. The theoretical fits represent results of numerical calculations using eq 1.

the EMA, ϵ_4 and ϵ_3 contain a number of unknown parameters, measurements of which require additional experiments involving multiple techniques.[27] Since such measurements are beyond the scope of this work, we consider only the effective values of ϵ_3 and ϵ_4, and not their constituent dielectric functions. In the following, we consider the observed details (the SPR angle, Γ_w, and $\Delta R/R$, in particular) of the SPR data and discuss the significance of the numerically obtained SPR parameters.

Effects of Au Nanoparticles on AET-Covered Au and Ag Substrates. The SPR characteristics for samples I and II are shown in Figure 5, parts A (Au/AET/Au) and B (Ag/AET/Au), respectively. The optical parameters for these samples are presented in the first six rows of Table 1. For the four-layer (0125) case, the three characteristic features, θ_0^p, Γ_w, and $\Delta R/R$, of the SPR plot (circles) are different in Figure 5, parts A and B. This is a result of the different values of ϵ_2 for the Au and Ag substrate films. These characteristic differences between the bare Au and Ag substrates are also manifested in Figures 6−8. A comparison of the plots with the triangle (five-phase, 01235 systems) in Figure 5, parts A and B, indicates that the AET considerably affects the SPR response of its underlying Ag in sample II, while the corresponding effect on Au in sample I are practically negligible. As shown in Table 1, both ϵ_{2r} and ϵ_{2i} of the Ag film undergo significant changes upon the adsorption of AET, but these changes are much smaller for the Au film. According to eq 9, this results in a noticeable change in Γ_w with the adsorption of AET on Ag, while the corresponding case for Au remains essentially unaffected. The different changes of ϵ_2 for Ag and Au also contribute to the different values of $\Delta R/R$ found for the five layer (01235) systems of the two substrates. Furthermore, the values of ϵ_3 are quite different for the AET layers on Ag and Au. The observations made here imply a stronger interaction of AET with Ag than with Au. In the formalism of eqs 2 and 9, the shift in the SPR angle (from θ_0^p to $\theta_0^{p'}$) due to the transition from systems 0125 to 01235 is given by[10]

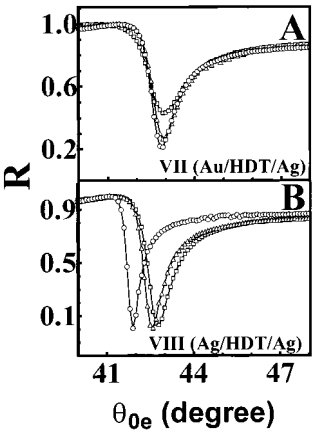

Figure 8. Experimental SPR data (symbols) and calculated fits (lines) to the data for Au (in A) and Ag (in B) substrates. The circles, triangles, and squares represent the four-phase (0125), five-phase (01235), and six-phase (012345) systems, respectively. The data in A and B refer to samples VII and VIII described in the Experimental Section, respectively. In both parts A and B, phase 3 represents a SAM of HDT, and phase 4 represents a layer of Ag nanoparticles. The theoretical fits represent results of numerical calculations based on eq 1.

$$\sin\theta_0^{p'} - \sin\theta_0^{p} = \Delta k_x^{(3)}/(\tilde{\omega}\sqrt{\epsilon_0}) \qquad (12)$$

According to eq 7, $\Delta k_x^{(3)}$ is proportional to the term (d_3/ϵ_3), and as indicated in Table 1, (d_3/ϵ_3) is noticeably larger for the Ag film in sample II than that for the Au film in sample I. Consequently, the AET-affected shift of the SPR angle occurs selectively for the Ag substrates.

All three SPR features, θ_0^p, Γ_w, and $\Delta R/R$, of Figure 5, part A, change considerably as we change over from the five-phase (triangles) to the six-phase (squares) systems. This is the case of the earlier mentioned Au nanoparticle enhanced SPR.[12−15] The corresponding nanoparticle mediated change for the Ag substrate (triangles- to squares-plots) in Figure 5B is relatively less drastic. According to the results in Table 1, neither ϵ_2 nor ϵ_3 experience any significant changes upon the adsorption of the Au nanoparticles, and this is true for both the Au and the Ag substrates. The thicknesses d_4 of the Au nanoparticle layer, as calculated from the fits of Figure 5, are also comparable for samples I and II. However, both ϵ_{4r} and ϵ_{4i} are different for the two samples and thus, give rise to different values of $\Delta k_x^{(4)}$ in the two cases. This accounts for the different nanoparticle induced SPR shifts in Figure 5, parts A and B, and according

to eq 9, the shifts are approximately characterized by the expression,

$$\sin \theta_0^{p''} - \sin \theta_0^{p'} = \mathrm{Re}[\Delta k_x^{(4)}]/(\tilde{\omega}\sqrt{\epsilon_0}) \qquad (13)$$

$\mathrm{Im}[k_x^{(4)}]$ affects the value of Γ_w through eq 10. Thus, the different values of $\mathrm{Im}[k_x^{(4)}]$ for samples I and II lead to different amounts of nanoparticle induced changes in the SPR widths for these samples. The corresponding changes in $\Delta R/R$ are also governed in a similar way by the different values of $\Delta k_x^{(4)}$ for the two samples.

The interactions between the SPP substrate and the adsorbed SAM seem to play a key role in the observed effects of layers 3 and 4 in Figure 5. The physical properties (charge distribution, orientation, packing density), and hence, ϵ_3 for the adsorbed AET layer on Au and Ag are different due to these interactions. The nanoparticle layers, chemically attached to such structurally and electronically different SAMs on Au and Ag are optically different with different values of ϵ_4 as we found for the two samples in Figure 5.[38] The changes in ϵ_3 are directly manifested in the SPR plots for the five-phase systems. The changes in ϵ_4 affect the behaviors of the six-phase SPR plots.

Effects of Au nanoparticles on HDT-Covered Au and Ag Substrates. The SPR characteristics samples III and IV, are shown in Figure 6. part A (Au/HDT/Au) and part B (Ag/HDT/Au), respectively. The optical parameters for samples III and IV are presented in the last six rows of Table 1. The four-phase (01235) base systems considered in Figures 5 and 6 represent two different sets of samples with somewhat different substrate thicknesses d_2. As a result, the SPR plots indicated by the circles in Figure 6, as well as their corresponding optical parameters listed in Table 1 are somewhat different from their counterparts considered for Figure 5. For the five-phase (01235) systems, the effects of HDT on the SPR resonance of Au (sample III, triangles in Figure 6, part A) are similar to those of AET (sample I, triangles in Figure 5, part A). As for the case of AET, the adsorption of HDT on Au also introduces only relatively small changes in the values of ϵ_{2r} and ϵ_{2i}. Furthermore, (ϵ_3/d_3), and $\Delta k_x^{(3)}$ are also comparable between samples I and III. Consequently, as in the case of sample I in Figure 5, part A, the SPR plots for sample III are also very similar between the four- and five-phase systems. For sample IV in Figure 6B, ϵ_{2r} and ϵ_{2i} of the Ag substrate undergo measurable changes with the adsorption of HDT, and lead to a nonzero $\Delta k_x^{(3)}$. The result is the observed shift in the SPR angle upon adsorption of HDT on Ag in Figure 6B. Apparently, these changes in ϵ_{2r} and ϵ_{2i} are not large enough to affect the width of the SPR plot. This is seen by comparing the amounts of changes in ϵ_2 that occur during the 0125-to-01235 transition in Figures 5B and 6B. For sample II in Figure 5B, both ϵ_{2r} and ϵ_{2i} change by at least a factor of 2 due to the adsorption of AET on Ag. For sample IV in Figure 6B, the corresponding changes due to the adsorption of HDT are considerably less drastic. Thus, according to eqs 10 and 11, the change of the SPR width, (from Γ_w(01235) to Γ_w(012345)), is more pronounced in Figure 5B than in Figure 6B.

For sample III in Figure 6, part A, $\theta_0^{p'}$, Γ_w, and $\Delta R/R$ of the five-phase (01235) structure are modified as the six-phase structure is formed upon the adsorption of Au nanoparticles. The situation (nanoparticle enhanced SPR shift) here is similar to that already observed for sample I in Figure 5, part A. For sample IV in Figure 6, part B, the transition from the five-phase to the six-phase systems also present results similar to those observed in the corresponding transition for sample II in Figure 5B. As in Figure 5, the values of ϵ_4 in Figure 6 are again different for the Au and Ag substrates. Thus $\Delta k_x^{(4)}$, and therefore, the nanoparticle induced changes of the SPR plot in Figure 6 are different between the Au and Ag substrates.

We note here that, in a previous paper, we presented preliminary SPR results for the multilayer combinations used in Figure 6.[15] However, the samples used in the present work are different from those used in ref 15. This is indicated in the different sets of values for ϵ_m and d_m, obtained in ref 15 and Figure 6 of the present work.

Effects of Ag Nanoparticles on AET Covered Au and Ag Substrates. The SPR characteristics for these systems, samples V and VI, are shown in Figure 7, parts A (Au/AET/Ag) and B (Ag/AET/Ag), respectively. The optical parameters for these samples are presented in the first six rows of Table 2. As expected, the SPR data for the four-phase (0125) and five-phase (01235) systems in Figure 7 are similar but, owing to the different substrate thicknesses, not identical to the corresponding data in Figure 5. This can be noted by comparing the circle- and triangle-plots in Figure 7, parts A and B, with those of Figure 5, part A (sample I) and part B (sample II), respectively. For the Au substrate, ϵ_2 and ϵ_3, in the four- and five-phase cases of sample V are comparable to those found in the corresponding cases of sample I. Similarly, for the Ag substrate, ϵ_2 and ϵ_3, for the four- and five-phase cases of sample VI are similar to those in the corresponding cases of sample II.

The results presented in Tables 1 and 2 indicate that the six-phase case for Ag nanoparticles in sample V is different from that for Au nanopartcles in sample I in three respects. First, as expected, ϵ_4 in the former mentioned case representing Ag nanoparticles is different from ϵ_4 in the latter case representing Au nanoparticles. Second, d_4 for sample V is considerably larger than that for sample I. Third, the adsorption of Ag nanoparticles in the case of sample V changes ϵ_2 of the Au substrate, while such a change is not observed when Au nanoparticles are adsorbed in the case of sample I. The last observation in particular, suggests the presence of interactions between layers 2 and 4 in sample V. Due to these differences in ϵ_2 (as well as in ϵ_4, d_4 and hence, in $k_x^{(4)}$) between samples I and V, the characteristic SPR parameters, $\theta_0^{p''}$, Γ_w, and $\Delta R/R$, of the two samples are also different between the six-phase systems of these samples. Comparing the six phase systems for samples II (Au/AET/Au) and VI (Au/AET/Ag), we find that the most noticeable difference between the two cases is in their values of ϵ_4. In particular, ϵ_{4r} for sample VI comes out to be positive in the results of the calculated fits presented in Table 2. A negative ϵ_{4r} implies that the nanoparticle layer of the metal retains the sign of its bulk dielectric function (which is the case for samples I−V and VII). On the other hand, a positive ϵ_{4r}, as found for sample VI, carries the sign of the dielectric function of the host medium in layer 4. Later in this paper, we show that the second situation also appears in the case of sample VIII. Furthermore, the thickness d_4 of the Ag nanoparticle layer of sample VI is found to be larger than the thickness of the Au nanoparticle layer of sample II. The different values of ϵ_4 and d_4 between samples II and VI are manifested in the different resonance angles and shapes of the six-phase SPR graphs for the two samples.

Effects of Ag Nanoparticles on HDT-Covered Au and Ag Substrates. The SPR characteristics for these systems, samples VII and VIII, are shown in Figure 8, partsA (Au/HDT/Ag) and B (Ag/HDT/Ag), respectively. The optical parameters for these samples are presented in the last six rows of Table 2. As expected, the SPR properties for the four-phase (0125) and five-

phase (01235) systems in Figure 8 are similar to the corresponding plots in Figure 6 (samples III and IV). This can be noted by comparing the circle- and triangle-plots in Figure 8, parts A and B, with those of Figure 6 parts A and B, respectively. For sample III in Figure 6, part A, $\theta_0^{p'}$, Γ_w, and $\Delta R/R$, change in going from the five-phase to the six-phase systems. The situation with sample VII in Figure 8, part A, is different, where only $\Delta R/R$ changes between the five- and six-phase systems, but $\theta_0^{p'}$ and Γ_w do not exhibit any significant changes in this transition. An examination of the optical parameters in Tables 1 and 2 indicates that apart from the expected variation of ϵ_4 between Au and Ag nanoparticles, a prominent difference between the SPR results for samples III and VII is in the values of ϵ_2 for the to six-phase cases. This difference is an indication of substrate-nanoparticles interactions in sample VII, which apparently are absent or weaker in sample III. It is possible that in the case of Figure 8, part A, these interactions act to impede the nanoparticle induced enhancement of SPR shift that was observed in Figure 6, part A.

For sample VIII in Figure 8, part B, the adsorption of Ag nanoparticles on Ag/HDT exhibits effects that are similar to those observed for Au nanoparticles adsorption on Ag/HDT of sample IV in Figure 6. Despite the larger value of d_4 in sample VIII, the particle induced shifts in the SPR angles and widths are similar for samples IV and VIII. Furthermore, neither ϵ_2, nor ϵ_3 for sample VIII displays any major changes in the (01235)-to-(012345) transition, and the same situation is found for sample IV. The last two observations indicate that the adsorption of Au or Ag nanoparticles on the Ag/HDT support has only minor effects on the initial SPR behavior of the five-phase system without such particles. We note, however, that like the case of sample VI, ϵ_{4r} for sample VIII also comes out to be positive in the calculated fits to the experimental data. In other words, within the range of materials considered in this work, the positive ϵ_{4r} appears to be specific to those systems where Ag nanoparticles are assembled on Ag substrates.

Possible Sources of Substrate−SAM−Particles Interactions. Let us summarize the main results of Figures 5−8 from the above discussion, and comment on the possible mechanisms for the effects observed in these figures. We have shown that in the absence of nanoparticles, both AET and HDT layers affect the SPP characteristics of Ag more than those of Au. This is also manifested in the parameters listed in Tables 1 and 2. Irrespective of its identity, the SAM layer upon its adsorption typically changes the dielectric function of the Ag substrate. On the other hand, such changes are considerably less noticeable for the Au substrates. To clarify this observation, we note that the SAM-induced change of the dielectric function of a metal substrate can be described in terms of changes in the surface work function of the metal caused by its adsorbates.[35−37] The latter phenomenon originates from adsorbate affected changes in the electron density of the metal surface, and is usually responsible for altering the free electron components of ϵ_{2r} and ϵ_{2i} of the metal. The incident photon energy (1.96 eV) used in the present work is below the d-band-to-Fermi level transition energies for Au (∼2.4 eV) and Ag (∼3.9 eV).[20] Therefore, ϵ_{2r} and ϵ_{2i} in the present experiments are dominated by their free electron components.[35] Consequently, any adsorption induced changes in these free electron dielectric functions of the substrate would have significant effects on the optical properties of these metals.[23] However, such adsorbate effects would depend on the ionic nature and strength of the SAM-substrate bond. From the considerations of electronegativity differences among S, Ag and Au, previous authors have noted that the Ag−S bond should be more ionic than the Au−S bond.[39,40] Therefore the SAM on Ag can affect the charge distribution at the adsorption site to a larger degree than it would do in the case of Au. According to this view, and in light of the above discussion, the dielectric function of Ag should be more affected than that of Au upon the adsorption of the SAMs. The results presented here are in agreement with this explanation.

In the systems explored here, the introduction of the nanoparticles does not generally change the dielectric function of the underlying SAM, but changes the dielectric function of the substrate in some cases (Au/AET/Ag, and Au/HDT/Ag, in particular). The dielectric function of the particle layer is sensitive to the chemical nature of the SAM (AET or HDT), and to some extent, also to the identity of the substrate metal. To explain these observations, we note a recent report, where the LSP resonance (dielectric function) of SAM-coated Ag nanoparticles is found to change as the SAM in the coating is changed.[38] Earlier experiments also report this type of effects of molecules attached to metal nanoparticles.[41,42] We propose that a similar environment-sensitivity is displayed by the dielectric functions of the Au and Ag nanoparticles in our present work. In this mechanism, apparently the SAM acts to perturb the electronic details of the adsorbed particles layer, while the dielectric function of the SAM itself is affected to a lesser degree. We also note that a charged nanoparticle forms its image in the metal substrate.[43] The local electric field of this image can provide additional contributions to the SAM induced changes in the dielectric function of the nanoparticle layer. At the same time, the image effect can also perturb the electronic details of the substrate and thus, the free electron part of ϵ_2. If this mechanism is operative, ϵ_2 of the substrate would change with the adsorption of nanoparticles, and the degree of such a change would depend on the metals used in layers 2 and 4.[44] Moreover, the presence of any roughness at the substrate surface would alter the image field of an ideal flat surface.[45] If the Au and Ag substrate surfaces are associated with different amounts of their characteristic roughnesses, the substrate−nanoparticle interactions based on the considerations of image fields would also be different for the two cases. These considerations are also consistent with the observations made in Figures 5-8.

We have used AET and HDT to test possible effects of the different types of chemical attachments between the nanoparticles and the spacer SAM. The results present suggestive evidence for the presence of such effects in the case of Au nanoparticles used in samples I−IV. For these samples, the values of ϵ_4 differ noticeably between the underlying SAMs of AET and HDT (although, no specific trends, linking the chemical nature of the nanoparticle−SAM bond to the occurrence of these changes can be identified at the present time). On the other hand, ϵ_4 for the Ag nanoparticles in samples V−VIII does not seem to change much between the two types of SAM attachments. A simple possible explanation for the observations made here follows from the consideration of surface charge density of the nanoparticles. This charge density contributes to interparticle interactions, and is likely to depend on the size of the particles.[38] The value of ϵ_M^{pl} and, hence, that of ϵ_4 for a given nanoparticle *M* also depends on its surface charge density.[20] At the same time, the net charge on a nanoparticle attached to a SAM would be sensitive to the electrostatic (for AET) or covalent (for HDT) nature of the particle−SAM bond. The Ag nanoparticles used in the present work are larger than the Au nanoparticles. This is seen in Tables 1 and 2 where d_4 for Ag nanoparticles in samples V−VIII (25−

32 nm) are larger than d_4 for their Au counterparts in samples I−IV (10−16 nm). If the surface charge per unit area of the larger Ag nanoparticle is smaller than that of the smaller Au nanoparticle, then this charge (and thus, ϵ_4) of Ag would be relatively less sensitive to the electronic nature of the bond formed by the attached SAM. The selective behavior of the Au nanoparticles in terms of their sensitivity to the type of SAM-attachment is consistent with this scenario.

5. Conclusions

In the present work, we have studied several aspects of metal nanoparticle enhanced SPR of Au and Ag films, probing in particular the conditions necessary to observe this enhancement, as well as the mechanism of this effect. We have demonstrated how the SPR enhancement can be observed for certain substrate/SAM/nanoparticles combinations using a six-phase multilayer SPR device. We have shown that the interactions in the multilayer structure play crucial roles in the generation and manifestation of this enhancement. The substrate−nanoparticle interactions are characterized by the interplay of SPP and LSP oscillations in the multilayer system. SAM-induced changes in the free electron properties of the substrate seem to have a considerable influence on the SPR characteristics of the system. Image field effects of charged nanoparticles also seem to play an important role in determining the optical response of the SPR device. Further SPR experiments, involving multiple wavelengths are necessary to completely understand the implications of the observations reported here. Particularly interesting in this regard would be experiments at incident wavelengths close to the LSP resonance of the nanoparticles. The LSP−SPP interactions are expected to be more pronounced at such wavelengths.[44] Likewise, the distance between the SPP substrate and the nanoparticle (the length and the orientation of the SAM molecule) can strongly affect the strength of these interactions.[46] Thus SPR experiments, using different lengths of the spacer SAM, near the wavelength of LSP resonance would be useful to probe further details of the LSP−SPP interactions.

Acknowledgment. This work was supported in part by the National Science Foundation. We thank Professor G. L'Espérance for allowing us to use his SEM facility.

References and Notes

(1) Brockman, J. M.; Nelson, B. P.; Corn, R. M. *Annu. Rev. Phys. Chem.* **2000**, *51*, 41.
(2) Quinn, J. G.; O'Neill, S.; Doyle, A.; McAtamney, C.; Diamond, D.; MacCraith, B. D.; O'Kennedy, R. *Anal. Biochem.* **2000**, *281*, 135.
(3) Xiao, C. D.; Sui, S. F. *Sens. Actuators, B* **2000**, *66*, 174.
(4) Melendez, J.; Carr, R.; Bartholomew, D.; Taneja, H.; Yee, S.; Jung, C. Furlong, C. *Sens. Actuators, B* **1997**, *39*, 375.
(5) Jung, L. S.; Campbell, C. T.; Chinowsky, T. M.; Mar, M. N.; Yee, S. S. *Langmuir* **1998**, *14*, 5636.
(6) Raether, H. *Surface Plasmons on Smooth and Rough Surfaces and Gratings*; Springer-Verlag: New York, 1988.
(7) Wang, S.; Boussaad, S.; Wong, S.; Tao, N. J. *Anal. Chem.* **2000**, *72*, 4003.
(8) Peterlinz, K. A.; Georgiadis, R. *Langmuir* **1996**, *12*, 4731−4740.
(9) de Bruijin, H. E.; Altenburg, B. S. F.; Kooyman, R. P. H.; Greve, J. *Opt. Commun.* **1991**, 425−432.
(10) Johansen, K.; Arwin, H.; Lundstrom, I.; Liedberg, B. *Rev. Sci. Instrum.* **2000**, *71*, 3530.
(11) Kolomenskii, A. A.; Gershon, P. D.; Schuessler, H. A. *Appl. Opt.* **2000**, *39*, 3314.
(12) Lyon, L. A.; Musick, M. D.; Natan, M. J. *Anal. Chem.* **1998**, *70*, 5177−5183.
(13) Lyon, L. A., Peña, D. J.; Natan, M. J. *J. Phys. Chem. B* **1999**, *103*, 5826−5831.
(14) Lyon, L. A.; Holliway, W. D.; Natan, M. J. *Rev. Sci. Instrum.* **1999**, *70*, 2076.
(15) Hutter, E.; Cha, S.; Liu, J.-F.; Park, J.; Yi, J.; Fendler, J. H.; Roy, D. *J. Phys. Chem. B* **2001**, *105*, 8.
(16) Fendler, J. H., Ed. *Nanoparticles and Nanostructured Films, Preparation, Characterization and Applications*; Wiley-VCH: Weinheim, 1998.
(17) Whitesides, G. M.; Laibinis, P. E. *Langmuir* **1990**, *6*, 87.
(18) Link, S.; El-Sayed, M. A. *J. Phys. Chem. B* **1999**, *103*, 8410.
(19) Mulvaney, P. *Langmuir* **1996**, *12*, 788.
(20) Krieibig, U.; Volmer, M. *Optical Properties of Metal Clusters*; Springer: Berlin, 1995.
(21) Wokaun, A. *Mol. Phys.* **1985**, *56*, 1−33.
(22) Azzam, R. M. A.; Bashara, N. M. *Ellipsometry and Polarized Light*; North-Holland: New York, 1989.
(23) Kurosawa, K.; Pierce, R. M.; Ushioda, S.; Hemminger, J. C. *Phys. Rev. B* **1986**, *33*, 789.
(24) Roy, D. *Appl. Spectrosc.* **2001**, *55*, 1046.
(25) Hutter, E.; Fendler, J. H.; Roy, D. *J. Appl. Phys.* **2001**, *90*, 1977.
(26) Roy, D. To be published.
(27) Aspnes, D. E. *Thin Solid Films* **1982**, *89*, 249−262.
(28) Chen, W. P.; Chen, J. M. *Surf. Sci.* **1980**, *91*, 601.
(29) Pockrand, I. *Surf. Sci.* **1978**, *72*, 577.
(30) Kretschmann, E. *Z. Phys.* **1971**, *241*, 313.
(31) Hirai, H.; Aizawa, H. *J. Colloid. Interface Sci.* **1993**, *161*, 471. Heand, S. M.; Grieser, F.; Barraclough, C. G. *J. Colloid Interface Sci.* **1983**, *93*, 545.
(32) Dobbs, D. A.; Bergman, R. G.; Theopold, K. H. *Chem. Eng. News* **1990**, *68*, 2.
(33) *Handbook of Chemistry and Physics*, 64th ed.; CRC Press, Inc.: Boca Raton, FL, 1983−1984.
(34) Bos, L. W.; Lynch, D. W. *Phys. Rev. B* **1970**, *2*, 4567.
(35) Walters, M. J.; Roy, D. *Appl. Spectrosc.* **1998**, *52*, 1554.
(36) Lovell, M. A.; Walters, M. J.; Roy, D. *Electrochim. Acta* **1998**, *43*, 2101.
(37) Lovell, M. A.; Walters, M. J.; Roy, D. *Phys. Chem. Chem. Phys.* **1999**, *8*, 1985.
(38) Malinsky, M. D.; Kelly, K. L.; Schatz, G. C.; Van Duyne, R. P. *J. Am. Chem. Soc.* **2001**, *123*, 1471.
(39) Bryant, M. A.; Pemberton, J. E. *J. Am. Chem. Soc.* **1991**, *113*, 8284.
(40) Schoenfisch, M. H.; Pemberton, J. E. *J. Am. Chem. Soc.* **1998**, *120*, 4502.
(41) Henglein, A. *J. Phys. Chem.* **1993**, *97*, 8457.
(42) Linnert, T.; Mulvaney, P.; Henglein, A. *J. Phys. Chem.* **1993**, *97*, 679.
(43) Roulet, B.; Saint Jean, M. *Am. J. Phys.* **2000**, *68*, 319.
(44) Takemori, T.; Inoue, M.; Ohtaka, K. *J. Phys. Soc. Jpn.* **1987**, *56*, 1587.
(45) Palasantzas, G. *J. Appl. Phys.* **1997**, *82*, 351.
(46) Kume, T.; Nakagawa, N.; Hyashi, S.; Yamamoto K. *Solid State Commun.* **1995**, *93*, 171.